Contents

1 Key Concepts

Note that Poincaré sections allow us to turn flows into maps!

We begin the class by exploring various chaotic maps, but a few characterizations that we've learned include:

Power Spectrum Typically periodic trajectories have very sharp peaks in their power spectrum, and quasi-periodic trajectories simply have peaks at frequencies that do not share a common factor. Chaotic trajectories have a broad power spectrum.

Lyapunov Exponents Lyapunov exponents let us quantify, for a given initial condition, how much phase space is expanding at that point. A positive Lyapunov Exponent implies nearby points diverge exponentially and are indicative of chaotic dynamics.

Entropy Kolmogorov Entropy is a measure of how many partitions a single partitioning in a partition maps to under a map. In non-chaotic dynamics, we would expect certain partitions to map strictly within themselves, but if this mixing is always positive, then the Kolmogorov Entropy is positive and suggests chaotic dynamics.

2 Lorenz Model

The Lorenz Model arises as an approximation to atmospheric flow, starting with the description of the simplest mode of a convection zone and dropping terms that represent higher harmonics. This gives the following system of equations

$$\begin{aligned} \dot{X} &= -\sigma(X - Y) \\ \dot{Y} &= rX - Y - XZ \\ \dot{Z} &= b(XY - Z) \end{aligned} \tag{1}$$

with parameters canonically set at $\sigma = 10, b = 8/3, r = 27 > 1$ (note that σ is 0.7 for an ideal gas, 1–4 for water and > 10 for oils). Note that the equations are dissipative, i.e. volumes in phase space shrink in dynamics. Note also that they are *autonomous* in that there is no explicit time dependence on the right hand side, a convenient property.

It turns out that the solutions to this system are chaotic, or in Lorenz's original terms "aperiodic." We do many demonstrations that are no longer accessible, including *strange attractors, Poincaré section* and *1D maps*.

The last is going to be covered in a later lecture, but in case I'm interested in simulating the former two, I look them up here (the website has discussions of these with the applets absent):

- Poincaré section examines the intersection of an orbit with a particular plane in phase space, e.g. $Z = 31$ is a common one. So we just simulate and examine every time that $Z = 31$ is crossed, exactly what (X, Y) are.
- Strange attractors are subsets of phase space with fractional dimension (fractals) that orbits at long times lie in.

3 Pendula

3.1 Ideal Pendulum

The ideal pendulum is given by EOM $\frac{\mathrm{d}^2\theta}{\mathrm{d}t^2} + \frac{g\sin\theta}{l} = 0$. We can plot phase space $(\theta, \omega = \dot{\theta})$ for solution trajectories. There are a few features of interest

- Fixed points — Two types, elliptic (stable but not asymptotically stable) and hyperbolic (unstable)
- Limit Cycles — Solution trajectories.
- Homoclinic orbits — Trajectories that connect the same hyperbolic fixed point. Heteroclinic orbits connect two different hyperbolic fixed points.

We can write down the Hamiltonian for this system $H = \frac{J^2}{2I} + Mgl(1-\cos\theta)$. The importance of being able to do is that phase space volume is preserved. What do we mean by this? Well, consider Hamilton's canonical equations

$$\begin{aligned} \dot{\theta} &= \frac{\partial H}{\partial J} = \frac{J}{I} \\ \dot{J} &= -\frac{\partial H}{\partial \theta} = -Mgl\sin\theta \end{aligned} \tag{2}$$

and if we define some phase space velocity $\vec{V} = \left(\dot{\theta}, \dot{J}\right)$ we can verify that $\nabla \cdot \vec{V} = 0$. In other words, no attractors in phase space can exist for a Hamiltonian system.

3.2 Dissipative Pendulum

New EOM is $\frac{\mathrm{d}^2\theta}{\mathrm{d}t^2} + \eta\frac{\mathrm{d}\theta}{\mathrm{d}t} + \frac{g}{l}\sin\theta = 0$. This creates a fixed point at $(0,0)$, asymptotically stable ("linearly stable" is his terminology), and $(\pi, 0)$ is suddenly linearly unstable, in that we will exponentially deviate from the point (before, we still periodically returned).

3.3 Driving + damping

Let's drive the pendulum and rescale variables to $\frac{\mathrm{d}^2\theta}{\mathrm{d}t^2} + \gamma\frac{\mathrm{d}\theta}{\mathrm{d}t} + \sin\theta = g\cos(\omega_D t)$. Under small angle approximation (small amplitude of solution and driving), we know how to solve this. What about with larger driving amplitudes though?

To handle this, we wish to solve numerically, which is much easier with an autonomous system than with an explicit time dependence. Thus, we introduce $\dot{\theta}_D = \omega_D$ and suddenly we can write

$$\begin{aligned}\dot{\theta} &= \omega \\ \dot{\omega} &= -\gamma\omega - \sin\theta + g\cos(\theta_D) \\ \dot{\theta}_D &= \omega_D\end{aligned} \tag{3}$$

This is a handy trick to get an autonomous system at the expense of an additional equation in the system of ODEs. We might also suspect that the behavior of the system changes when we get an extra dimension of phase space.

Well, let's start by observing that $\vec{\nabla}\cdot\vec{v} = -\gamma$ so phase space volumes contract. This might naively lead us to conclude that any volume of initial conditions must contract to a point, but we mustn't be hasty; the Lorenz model also has contracting phase space volumes. Instead, we know that we might approach a limit cycle in a way such that while the overall phase space contracts, the space might "stretch" along some dimensions and contract in others such that chaotic dynamics are observed! The demonstrations illustrating this are broken, but we will definitely simulate this.

4 Nonlinear Oscillators

4.1 Van der Pol Oscillator

Consider the following model of a harmonic oscillator to include a non-linear damping. Damping is negative at small amplitudes to model local instability, but is positive for larger amplitudes; we thus expect the system to have some limit cycles where the average damping vanishes. The EOM is

$$\ddot{x} - \gamma(1 - x^2)\dot{x} + x = g\cos(\omega_D t) \tag{4}$$

4.1.1 Small γ, secular perturbation

Let's first look at oscillations with no driving, $g = 0$. We return to the second order EOM for this. The natural starting point is to also examine for small γ and try Lindstedt-Poincaré perturbation theory (also called secular perturbation theory) on

$$\ddot{x} + x = \gamma(1 - x^2)\dot{x} \tag{5}$$

We begin with the $\gamma = 0$ solution, which is just $x(t) = ae^{it+\phi}$. Then, by secular perturbation theory[1], when $\gamma \neq 0$, we can substitute $x(t) = A(t)\cos(t) + \gamma x_1 + \dots$ and also expect $A(t)$ to be some slow-varying function such that $\dfrac{\mathrm{d}^n A(t)}{\mathrm{d}t^n} \sim \gamma^n$ (this is introducing a second slow time scale, characteristic of secular perturbation theory

[1] We learned as *Lindstedt-Poincaré* in 106, but this seems to differ slightly; instead of setting up this slowly varying timescale as below, we tend to set $s = \omega t$ and expand $\omega = 1 + \epsilon\omega_1 + \dots$.

apparently) and collect $O(\gamma^1)$ terms in the ODE to obtain

$$\begin{aligned}\frac{\mathrm{d}^2}{\mathrm{d}t^2}\left[A\cos(t)+\gamma x_1\right]+A\cos(t)+\gamma x_1 &= \gamma(1-A^2\cos^2(t))\frac{\mathrm{d}}{\mathrm{d}t}(A\cos(t))\\ -2\sin(t)\frac{\mathrm{d}A}{\mathrm{d}t}+\gamma\frac{\mathrm{d}^2x_1}{\mathrm{d}t^2}+\gamma x_1 &= -\gamma A\sin(t)+\gamma A^3\underbrace{\cos^2(t)\sin(t)}_{\frac{\sin(t)}{4}+\frac{\sin(3t)}{4}}\\ \gamma\left(\frac{\mathrm{d}^2x_1}{\mathrm{d}t^2}+x_1\right) &= -\gamma A\sin(t)+\gamma A^3\frac{\sin(t)}{4}+2\sin(t)\frac{\mathrm{d}A}{\mathrm{d}t}+O(\sin(3t))\end{aligned} \tag{6}$$

where we don't care about the $\sin(3t)$ term since it doesn't drive x_1 on resonance. On the other hand, we require the remaining term vanish, which implies that

$$2\frac{\mathrm{d}A}{\mathrm{d}t}=\gamma A-\frac{\gamma A^3}{4}=\gamma\frac{A(4-A^2)}{4} \tag{7}$$

off of which we can read that any initial $A>0$ tends to grow until $A=2$, asymptoting at $x(t)=2\cos(t)$.

4.1.2 Large γ

For large γ, let's stick to driving $g=0$ and go to a slightly unconventional choice of phase space variables, namely

$$\dot{y}=\ddot{x}-\gamma(1-x^2)\dot{x}=-x \tag{8}$$

$$\dot{x}=y+\gamma\left(x-\frac{x^3}{3}\right) \tag{9}$$

We then rescle $y\to\gamma Y, t\to\gamma T, x\to X$ and introduce $\eta=\gamma^{-2}$ and obtain

$$\eta\frac{\mathrm{d}X}{\mathrm{d}T}=Y+\left(X-\frac{X^3}{3}\right) \tag{10}$$

$$\frac{\mathrm{d}Y}{\mathrm{d}T}=-X \tag{11}$$

and for large γ we now have small η. We first find that $\eta = 0$ is inconsistent; the first equation reduces to $Y = -\left(X - \frac{X^3}{3}\right)$, predicting a minimum of $Y = -\frac{2}{3}$ while the latter suggests $Y \to 0$ strictly decreasing-ly, contradictory. However, we can still analyze qualitatively what happens for small η, an orbit that comprises two pieces

- $Y + \left(X - \frac{X^3}{3}\right)$ is small, so $Y \simeq \frac{X^3}{3} - X$ and Y, X change on timescales $O(1)$.
- $Y + \left(X - \frac{X^3}{3}\right) \gg \eta \frac{\mathrm{d}X}{\mathrm{d}T}$, then X changes very rapidly over timescale $O(\eta^{-1})$, and since $\frac{\mathrm{d}Y}{\mathrm{d}T} \sim O(1)$ we can treat Y to be constant.

This breaks down to the orbit following $Y = \frac{X^3}{3} - X$ until reaching an extremum, at which point $\frac{\mathrm{d}X}{\mathrm{d}T} = 0$ and $Y + \left(X - \frac{X^3}{3}\right) \gg \eta \frac{\mathrm{d}X}{\mathrm{d}T}$, and suddenly we evolve at constant Y until we hit another point on the $Y = \frac{X^3}{3} - X$ curve. The picture is then of following a cubic on $X < -1, X > 1$ and jumping from $\left(-1, \frac{2}{3}\right) \to \left(2, \frac{2}{3}\right)$ and from $\left(1, -\frac{2}{3}\right) \to \left(-2, -\frac{2}{3}\right)$ (the constant Y portions of the curve).

This analysis allows us to compute $\dot{x} = v = \gamma\left[Y - \left(-X + \frac{X^3}{3}\right)\right]$ as the difference between $\frac{X^3}{3}$ the cubic and Y which tracks the cubic for $X < -1, X > 1$ and is constant during the jumps. We can simulate via Mathematica, and verify the shape of the trajectory.

This shows that there are free oscillations at any given γ.

4.2 Driven Oscillations: Frequency Locking

In general, when one drives an oscillator, one can either observe oscillations at both the free and driving frequency (in which case the power spectrum would show signatures at both frequencies), or we would see only a single frequency (and maybe harmonics). The latter case is called *frequency locking*, when the driving frequency

locks the free oscillation to some fixed frequency. The former case, when the driving and free oscillations are in an irrational ratio, is considered *quasiperiodic*, because the sum of the two frequencies never repeats.

Another way to define frequency locking is that while some parameters of the problem (e.g. drive amplitude, dissipation) are varied, all peaks in the power spectrum must remain fixed for some non-zero parameter space. If the frequency is not locked, at least some peaks should vary continuously as parameters are varied continuously. It turns out that frequency locking occurs for the vDP oscillator for high drive amplitude and small frequency differences, which is generally true.

The basic idea behind analyzing frequency locking (beyond the scope of this class) is to take equation of motion

$$\ddot{x} + x = \gamma(1 - x^2)\dot{x} + g\cos(\omega_D t) \tag{12}$$

and substitute $\omega_D = 1 + \gamma\Delta$ and $g = 2\gamma F$ again in the $\gamma \ll 1$ limit, so weak driving near resonance. Performing the same secular perturbation theory (I concede, it is easier to use $x(t) = A(t)e^{it} + c.c. + \epsilon x_1$ here than cosines) and write driving term $\epsilon F e^{i\Delta\epsilon t}e^{it}$, we obtain that killing the secular term requires

$$\frac{\mathrm{d}A}{\mathrm{d}t} = \frac{\gamma}{2}\left(A - |A|^2\right) - \gamma\frac{i}{2}Fe^{i\Delta\epsilon t} \tag{13}$$

then we can make the substitution $\tilde{A} = Ae^{-i\Delta\epsilon t}$ which yields

$$\frac{\mathrm{d}\tilde{A}}{\mathrm{d}t} + i\gamma\Delta\tilde{A} = \frac{\gamma}{2}\left(\tilde{A}(1 - \left|\tilde{A}\right|^2) - iF\right) \tag{14}$$

upon which whether locking happens boils down to the nature of algebraic solutions to $\tilde{A}$ above. A stable *fixed point* yields a locked solution (harmonics nearby tend to disappear) while stable *limit cycles* produce unlocked solutions (two frequencies), since the Poincaré-Bendixson theorem tells us that no other asymptotic long term dynamics are possible. Unstable solutions are uninteresting; if both stable fixed and limit cycles exist then both locked and unlocked dynamics can manifest. The

remainder of this is omitted.

It turns out that the vDP oscillator does not exhibit chaos.

4.3 Duffing Oscillator

The Duffing Oscillator, given by potential

$$V(x) = \pm\frac{1}{2}x^2 + \frac{1}{4}x^4 + \frac{1}{4} \tag{15}$$

and EOM

$$\ddot{x} + \gamma\dot{x} \pm x + x^3 = g\cos(\omega_D t) \tag{16}$$

does exhibit chaos for both signs apparently!

5 One Dimensional Maps

Let's consider an arbitrary system

$$\dot{U} = f(U|r) \tag{17}$$

with r some control parameters and U a vector of phase space coordinates. We have studied solely such systems that are

autonomous no time appears on RHS

deterministic no stochasticity in EOM

dissipative volumes in phase space shrink, giving attractors

The structure of the phase space is of smooth *vector fields* in $\mathbb{R}^N$, and the solution $U(t)$ is called a *flow*. Casting in this language gives us strong categorizations of what is/isn't possible such as the *Poincaré-Bendixson Theorem*.

5.1 Maps

In a map, we study an analogous system to(17) but with a discrete timestep $U_{n+1} = F(U_n|r)$. The effect of the evolution on volumes in phase space is then given by the Jacobian

$$J = \left| \frac{\partial^2 (F^{(i)})}{\partial (U^{(j)})^2} \right| \tag{18}$$

If $J = 1$ then the map is called *volume preserving*, otherwise *dissipative*. A few ways to map flows to maps:

- Integrate the flow for $n\tau$ with τ some fixed time interval.
- $N - 1$ dimensional Poincaré section.

Some notes about flows:

- Conventionally we scale maps to map $[0, 1]$ onto itself.
- Successive iterations of the map are notated $F^n(x_0)$.
- Defining $x_f : F(x_f) = x_f$ fixed point, we can also ask the whether the fixed point is stable. The usual technique is to linearize the map about $x = x_f + \delta x$ and compute the Taylor expansion $\delta x_{n+1} = F'(x_f)\delta x_n$. We thus observe stability if $F'(x_f) < 1$ and instability for the opposite.

5.1.1 Bifurcations

Suppose we have a map $F(x|a)$ with some parameter a. Then, as a is varied, it is possible that the long time solution of the map changes. These changes are called bifurcations. We depict bifurcations by plotting long time stable $F^k(x|a)$ as a function of a. For instance, a period 2 orbit that is exhibited for some value of a is plotted as two points $(a, x_1), (a, x_2)$ $(F^2(x_1) = F(x_2) = x_1)$. Regions of a for which a fixed point orbit exists show up as a single curve, and regions with chaotic dynamics show up as a continuum of points.

To be able to better describe these chaotic regions, we look to a statistical description. The *invariant measure* is the probability density of x values that an orbit visits. We begin by defining the *measure*.

$$\rho(x, x_0)\,\mathrm{d}x = \lim_{N\to\infty} \frac{1}{N} \times n(x, x_0) \tag{19}$$

where $\rho(x, x_0)$ is the density of points with initial condition x_0 and $n(x, x_0)$ is the number of times the orbit visits $[x - \mathrm{d}x, x + \mathrm{d}x]$ out of N iterations.

It turns out that this measure $\rho(x, x_0)$ doesn't actually depend on x_0 for almost all choices of x_0, so we define $\rho(x)$ the invariant measure of our attractor. Sometimes the invariant measure can be constructed directly from its definition

$$\rho_n(y) = \rho_{n+1}(y) = \int \mathrm{d}x\ \delta\left[y - F(x)\right] \rho_n(x) \tag{20}$$

5.1.2 Lyapunov Exponents

We can better quantify "sensitive depndence on initial conditions" by Lyapunov Exponents. We demand that for some pair of initial conditions $x_0, x_0 + \epsilon$ for the distance to grow as $|\delta x_n| = \epsilon e^{n\lambda(x_0)}$. $\lambda(x_0)$ is the Lyapunov Exponent

$$\lambda(x_0) = \lim_{n\to\infty}\lim_{\epsilon\to 0}\log\left|\frac{F^n(x_0+\epsilon) - F^n(x_)}{\epsilon}\right| = \lim_{n\to\infty}\frac{1}{n}\log\left|\frac{\mathrm{d}F^n(x_0)}{\mathrm{d}x_0}\right| \tag{21}$$

For systems with ergodic invariant measure, λ is independent of x_0, so we will call λ *the Lyapunov Exponent of the map*. Note that the derivative is of the n-th iteration, and it turns out that

$$\lambda = \lim_{n\to\infty}\frac{1}{n}\log\left|\frac{\mathrm{d}F^n(x_0)}{\mathrm{d}x_0}\right| = \lim_{n\to\infty}\frac{1}{n}\log|F'(x_{n-1})F'(x_{n-2})\dots F'(x_1)F'(x_0)| = \langle\log|F'|\rangle \tag{22}$$

A positive λ means that closely spaced initial conditions diverge exponentially, which is a signature of chaos and often used as a definition thereof.

6 Two Dimensional Maps

One-dimensional maps are a restricted view of most dynamical systems, which cannot simply be iterated in reverse to find the initial condition (many non-invertible systems). On the other hand, integrating most dynamical equations in reverse can yield the preimage of a trajectory, which leads us to *two*-dimensional maps as a faithful representation of a smooth flow in 3D phase space. Here, we will investigate four examples of 2D maps.

6.1 Henon Map

Consider the Henon map, which iterates

$$x_{n+1} = y_n + 1 - ax_n^2 \qquad\qquad y_{n+1} = bx_n \tag{23}$$

The Jacobian is $J = \begin{vmatrix} -2ax_n & 1 \\ b & 0 \end{vmatrix} = |b|$, so for $b = 1$ the map is area preserving and for $b < 1$ the map is dissipative, where areas in phase space contract. This is where the chaos lives. To get some intuition about what the strongly dissipitive limit looks like, we can substitute $x_{n+1} = bx_{n-1} + 1 - ax_n^2$ which for $b \to 0$ is simply $x_{n+1} \approx 1 - ax_n^2$ the quadratic map we studied in the previous chapter (that I ignored).

Canonically chosen values are $a = 1.4, b = 0.3$.

6.2 Baker's Map

The Baker's map is given by the mapping

$$x_{n+1} = \begin{cases} \lambda_a x_n & y_n < \alpha \\ (1-\lambda_b) + \lambda_b x_n & y_n > \alpha \end{cases} \qquad y_{n+1} = \begin{cases} y_n/\alpha & y_n < \alpha \\ (y_n - \alpha)/\beta & y_n > \alpha \end{cases} \tag{24}$$

with $\beta = 1 - \alpha, \lambda_a + \lambda_b \leq 1$, so points in 2D phase space on either side of the $y = \alpha$ boundary are mapped to $x < \lambda_a, x > 1 - \lambda_b$ respectively. Then when $\lambda_a + \lambda_b < 1$, the total phase space area decreases and the map is *dissipative*. Qualitatively, we see

that the number of vertical striations increases with increasing iterations, specifically with the nth iteration we have $\binom{n}{m}$ stries of width $\lambda_a^m \lambda_b^{n-m}$.

Note that for the Bakers' map, the attractor is *hyperbolic* in that, crudely, at each point phase space both an expanding and contracting direction can be defined such that the directions vary continuously across the map and are bounded to be nonzero. In the case of the Bakers' map, the map is expanding in the y direction and contracting in the x across the entire map and so is hyperbolic. Not many maps/flows are hyperbolic, but many useful properties can be proven in such cases.

6.3 Other 2D maps

Other interesting maps are the Duffing and the Kaplan-Yorke, also simulated in our tests. We are unable to simulate the Baker's Map because its chaos relies on how regions of phase space map and our simulation module is not presently powerful enough to handle this.

7 Power

One interesting potential criterion for chaos is the power spectrum of a signal. Periodic/quasidperiodic signals all give peaks at countably many frquencies, while chaotic dynamics tend to yield broad bands in the power spectrum. Nonetheless, due to observation time constraints and their impact on observed power spectra, we must characterize the impacts of these phenomena first before using this as a solid criterion.

If we had an infinite time series $y(t)$, then the power spectrum of the signal is given simply by $P(\omega) \propto |y(\omega)|^2$, and our above analysis would make sense. However, realistically we have a signal y_i measured in discrete intervals over a finite interval $t \in [0, T]$, so the power spectrum is estimated by the Fourier series

$$\tilde{y}_k = \sum_{j=0}^{N-1} y_j \exp\left(\frac{2\pi i j k}{N}\right) \tag{25}$$

$$= \sum_{j} y(t_j) \exp\left(i\omega_k t_j\right) \tag{26}$$

and the power spectrum is given

$$P(\omega) \simeq \frac{1}{N^2} \begin{cases} |\tilde{y}_0|^2 & \omega = 0 \\ \left|\tilde{y}_{N/2}\right|^2 & \omega = \dfrac{\pi N}{T} \\ \left(|\tilde{y}_k|^2 + |\tilde{y}_{N-k}|^2\right) & \end{cases} \tag{27}$$

To figure out how well this power spectrum estimates the real power spectrum of some signal $y(t)$ that we sample with y_i, we can realize that our $\tilde{y}_k$ can be written in terms of $y(t)$ like

$$\tilde{y}(t) = [(y(t) \times H(t, T)) * S(t, T)] \times S(t, \Delta) \tag{28}$$

with $S(t, \tau)$ a Dirac comb with period τ and H the tophat function. The convolution represents the periodic assumption, and the product by the Dirac comb samples in

intervals of $\Delta = \frac{T}{N}$. But we can compute the FT of the above function to be

$$\tilde{y}(\omega) \propto \left[\left(\tilde{y}(\omega) * \tilde{H}\left(\omega, \frac{2\pi}{T}\right)\right) \times S\left(\omega, \frac{2\pi}{T}\right)\right] * S\left(\omega, \frac{2\pi}{\Delta}\right) \tag{29}$$

where we know that the FT of H is just a sinc function with width $\sim 1/T$ and falls off like ω^{-1}. The prescription is thus "Take the ideal FT, broaden with a sinc, sample every $2\pi/T$, then convolve to periodically repeat." This last convolution means that all higher frequencies will just be aliased back into the Nyquist range $\pm\pi/\Delta$.

It is also possible to convolve by a less sharp windowing function than H, which means that the FT falls off faster and the ideal power spectrum is less broadened.

8 Lyapunov Exponents

Lyapunov exponents describe how quickly nearby trajectories diverge. In one dimension, it was just $\left\langle \log \left| \frac{\mathrm{d}f}{\mathrm{d}x} \right| \right\rangle$. Let's generalize this.

8.1 The Jacobian

Consider the map $U_{n+1} = F(U_n)$. We want to know how different the trajectory is starting from U_0 and from some small change. This is described by the Jacobian matrix

$$K_{ij}(U_n) = \left. \frac{\partial F_i}{\partial U^{(j)}} \right|_{U=U_n} \tag{30}$$

and so if two trajectories are at $U_n, U_n + \epsilon_n$ then $\epsilon_{n+1} = \mathbf{K}(U_n)\epsilon_n$.

For continuous systems $\dot{U} = f(U)$, then we have instead $\frac{\mathrm{d}\epsilon}{\mathrm{d}t} = \mathbf{K}(\mathbf{U})\epsilon$ for $K^{(ij)} = \frac{\partial f_i}{\partial U^{(j)}}$. But if we introduce a new matrix $\mathbf{M}$ satisfying $\frac{\mathrm{d}\mathbf{M}}{\mathrm{d}t} = \mathbf{K}(U(t))\mathbf{M}$, then we have

$$\frac{\partial U^{(i)}(t)}{\partial U^{(j)}(t_0)} = M_{ij}(t, t_0) \tag{31}$$

8.2 Oseledec's Multiplicative Ergodic Theorem

Developing the above formalism lets us introduce the concept of how quickly a particular area of phase space is expanding in all dimensions. Denote λ_i to be the exponential rate of growth along dimension i (e.g. in one dimension, $\lambda = \left\langle \log \left| \frac{\mathrm{d}f}{\mathrm{d}x} \right| \right\rangle$).

Oseldec's Multiplicative Ergodic Theorem lets us quantify this:

For almost any initial point $U(t_0)$, there exists an orthonormal set of vectors $v_i(t_0)$ spanning the phase space such that

$$\lambda_i = \lim_{t \to \infty} \frac{1}{t - t_0} \log |\mathbf{M}(t, t_0) v_i(t_0)| \tag{32}$$

exists. Moreover, for an ergodic system[2], these λ_i do not depend on the choice of initial point $U(t_0)$.

The λ_i can be calculated as the log of the eigenvalues of $\sqrt{\mathbf{M}^T\mathbf{M}}$.

This λ_i quantifies the exponential rate of expansion along a given v_i. The inspiration for the calculation of the λ_i can be observed to be taken from the SVD of $\mathbf{M} = \mathbf{WDV}^T$.

The best way to compute Lyapunov exponents is to use a sort of Gram-Schmidt algorithm, where we start with three orthonormal vectors, evolve, then renormalize. This procedure can be imagined to converge on the correct v_i, and their corresponding λ_i can be determined by seeing how much stretching occurs upon evolution.

The defining signature of chaos can be considered a positive Lyapunov exponent. On the other hand, fixed pointts have all negative exponents, limit cycles have one zero exponent (along the cycle) and m-frequency quasiperiodic orbits have m zero eigenvalues, along the m directions. Recall that a quasiperiodic orbit can be thought of as an m-torus in phase space, and so at any point, there are m many directions that we can go in to stay on the torus.

8.3 Lyapunov Exponents for the Lorenz Model

Recall the Lorenz equations are given

$$\dot{X} = -\sigma(X - Y) \tag{33}$$

$$\dot{Y} = rX - Y - XZ \tag{34}$$

$$\dot{Z} = XY - bZ \tag{35}$$

[2]Ergodic means that over time, the system visits all points in phase space.

A small perturbation $\epsilon = (\delta X, \delta Y, \delta Z)$ evolves by the linearized equations

$$\delta\dot{X} = -\sigma(\delta X - \delta Y) \tag{36}$$

$$\delta\dot{Y} = r\delta X - \delta Y - (\delta X\, Z + X\, \delta Z) \tag{37}$$

$$\delta\dot{Z} = \delta X\, Y + X\, \delta Y - b\, \delta Z \tag{38}$$

or

$$\frac{\mathrm{d}\epsilon}{\mathrm{d}t} = \underbrace{\begin{bmatrix} -\sigma & \sigma & 0 \\ r - Z & -1 & -X \\ Y & X & -b \end{bmatrix}}_{\mathbf{K}} \epsilon \tag{39}$$

where $\mathbf{K}$ is the Jacobian.

To calculate the Lyapunov exponents, we can simply start with the three basis vectors $\hat{\imath}, \hat{\jmath}, \hat{k}$, then we evolve and project as per the above prescription.

9 Entropy

In the limit of equally likely outcomes, entropy is defined as the log of the number of such outcomes, also associated with the "information capacity." For N possible microstates with different probabilities p_i, we can generalise entropy to be

$$I = S = \langle \log p_i \rangle = -\sum_{i=1}^{N} p_i \log p_i \tag{40}$$

with p_i the probability the microstate is occupied.

9.1 In Dynamical Systems

In a dynamical system, we partition its phase space V into N boxes B_i, and if we define some probability density $\rho(\vec{x})$ with $\vec{x} \in V$, then the probability of being in box B_i is simply $p_i = \int_{B_i} \rho(\vec{x}) \mathrm{d}x$, and the entropy of this partitioning $\{B_i\}$ is written

$$S = -\sum_{i=1}^{N} p_i \log p_i \tag{41}$$

While this definition is not inherently helpful without specifying the $\{B_i\}$, how it scales is of interest to us in two ways:

Information Density — How does S scale with decreasing partition size B_i.

Kolmogorov Entropy — How does S evolve in time?

9.2 Kolmogorov Entropy

S's evolution in time directly tells us about the amount of uncertainty/information in the dynamical system over time. Suppose we know the initial conditions to some finite accuracy, then the Kolmogorov Entropy of the system tells us how our prediction of some future state degrades due to "sensitive dependence on initial conditions."

Suppose we choose some $\{B_i\}$, then for any map M we can also compute the pre-image $\left\{M^{-1}B_i\right\}$, then we can choose a partition of $B_{ij} = B_i \cap M^{-1}(B_j)$, a much finer partitioning. Call this partitioning β_1 (since we are examining one preimage prior). The entropy of this partitioning is $S(\beta_1) = -\sum_{ij} p_{ij} \log p_{ij}$.

The Kolmogorov entropy, the change in entropy as we increasingly fine grain (as we look at pre-images for multiple steps back), is given

$$K = \lim_{m\to\infty} \frac{1}{m} S(\beta_m) \tag{42}$$

A positive K can be used to define chaos. This is because K has positive growth, i.e. partitions are refined indefinitely, only when nearby trajectories diverge (moreover, they diverge an amount that does not asymptotically vanish, else they could just approach a limit configuration).

It turns out that the Kolmogorov entropy K is bounded by the sum of the positive Lyapunov exponents $K \leq \sum_{\lambda^i>0} \lambda^i$.

10 Fractional dimensions

Chaotic attractors are in general not a neat subspace of their embedded space, not usually an area or a curve but something in between. We can characterize this by a fractional dimension, and we call the structure a fractal.

10.1 Capacity

The *capacity* of a set (incidentally often equal to the Hausdorff dimension, discussed below) can be defined as follows. Consider if we have a set in m dimensional space, then we tile the space with cubes of side length ϵ. The capacity is defined as

$$D_C = \lim_{\epsilon \to 0} \frac{\log N(\epsilon)}{\log(\epsilon^{-1})} \tag{43}$$

where $N(\epsilon)$ is the number of cubes containing a point in the set.

We apply this to the Cantor set, where we successively remove the middle third of every line segment still remaining, starting with the segment $[0, 1]$. If we choose $\epsilon_m = 3^{-m}$, then we note that at every choice of ϵ_m, exactly 2^m of them contain points from the Cantor set. Thus, the capacity is computed to be $D_C = \lim_{m \to \infty} \frac{m \log 2}{m \log 3} = \frac{\log 2}{\log 3}$

To apply this concept to a dynamical set is non-trivial: generally, iterating for too long saturates the ϵ partition, and moreover small perturbations in initial conditions can drastically change which boxes contain points. Generally, $N(\epsilon)$ will be plotted as a function and only over some range (for a given data set) will the plot be linear.

Moreover, in many maps (e.g. the Hénon), a phenomenon called *lacunarity* means that the estimate of dimension *oscillates* as we decrease ϵ! Ruff tuff stuff.

10.2 Hausdorff dimension

The Hausdorff dimension D_H is often equal to the capacity D_C, but occasionally provides more sensible answers.

Cover the set with m-cubes of *variable* edge length $l_i \leq \epsilon$. Define then a partition function

$$\Gamma(d, \epsilon) = \inf \sum_i l_i^d \tag{44}$$

then there is a D_H such that $\Gamma(d) = \lim_{\epsilon \to 0} \Gamma(d, \epsilon) = \begin{cases} 0 & d > D_H \\ \infty & d < D_H \end{cases}$

Clearly, if we choose $l_i = \epsilon$ we recover D_C, but some trickier problems may require more clever choices.

10.3 Generalized dimensions

Since phase space can be very large compared to the size of the attractor, it's easy for the above techniques to yield difficult-to-interpret results, as they concern the entire space rather than the nature of the attractor itself. *generalized dimensions* are an attempt to remedy this, and again there are two definitions:

Box Counting Approach Cover the attractor with boxes of size ϵ and $p_i = N_i/N$ the number of boxes in box i out of a total of N points in the attractor. The q-th generalized dimension is then

$$D_q = \lim_{\epsilon \to 0} \frac{1}{q-1} \frac{\log \sum_i p_i^q}{\log \epsilon} \tag{45}$$

Partition Function Approach Similar to the Hausdorff dimension, we can cover the set with m-boxes of size $l_i \leq \epsilon$, then define partition function

$$\Gamma(q, \tau, \epsilon) = \begin{cases} \inf \sum_i \frac{p_i^q}{l_i^\tau} & q \leq 1, \tau \leq 0 \\ \sup \sum_i \frac{p_i^q}{l_i^\tau} & q \geq 1, \tau \geq 0 \end{cases} \tag{46}$$

and there exists a $\tau(q)$ such that $\Gamma(\tau < \tau(q)) = 0$ else infininty. The q-th generalized dimension is then $D_q^H = \dfrac{\tau(q)}{q-1}$.

Generally the D_q are constant, but sets for which they are not constant yield *multifractals*.

A few special values of q are:

- $q = 0$ — This reproduces the capacity/Hausdorff dimension.
- $q = 1$ — This gives $D_1 = \lim_{\epsilon \to 0} \dfrac{-\sum_i p_i \log p_i}{-\log \epsilon}$ which tells us how information scales with box size, so we call D_1 the information dimension.
- $q = 2$ — This yields $D_2 = \lim_{\epsilon \to 0} \dfrac{\log \sum_i p_i^2}{\log \epsilon}$ which tells us the probability that two points lie within cells of length ϵ, so we call this the *correlation dimension*

10.4 Lyapunov Dimension

Can we construct a characterization of the attractor, its dimension, from analysis of the dynamics, which exhibit the attractor? More precisely, can we find a link betwween the Lyapunov exponents and the dimension? Kaplan-Yorke proposed

$$D_L = \nu + \frac{1}{|\lambda_\nu + 1|} \sum_{i=1}^{\nu} \lambda_\nu \tag{47}$$

and conjectured that $D_L = D_1$, the unproven *Kaplan-Yorke conjecture*.

11 Multifractals, chaos

11.1 $f(\alpha)$

For many attractors, we can compute the measure of the attractor $\rho(x)$. In the case of $a = 4$ for the quadratic map, we obtain measure

$$\rho(x) = \frac{1}{\pi\sqrt{x(1-x)}} \tag{48}$$

which has $x^{-1/2}$ at the endpoints. But in general, the singularities exhibit a more complicated distribution, which generally is characterized as fractals with different measure singularities... let's see what this means!

Consider covering the attractor with an $m$box with side length l. The p_i of each box can be described in terms of l^{α_i} with α_i describes the measure of the singularity. We then define $f(\alpha)$ to be the dimension of points with singularity measure $\alpha_i = \alpha$. In other words, the number of points we expect to see at points with singularity measure α should scale like $l^{-f(\alpha)}$.

Thus, for our above example, the endpoints have a probability density $\rho(x) \propto l^{-1/2}$ and have an associated probability measure $\int_0^l x^{-1/2}\,\mathrm{d}x = x^{1/2}$ and corresponds to $\alpha = 1/2$. Thus, $f(1/2) = 0, f(1) = 1$ since the rest of the interval has unit probability measure.

11.2 Relationship to D_q

Note that D_q is a weighted sum over boxes of p^q with p being the measure associated with the box. However, the scaling of the probability measure with box size is described by the pointwise dimension α. Thus, we see that these should be related.

Recall that D_q is defined as a sum of $\sum_i p_i^q$ over the boxes $\{B_i\}$. Let's suppose we have a more general attractor that exhibits a continuous range of α with weights

$w(\alpha)$, then we can re-express the above sum as

$$p_i^q = \int_{B_i} l^{q\alpha} \mathrm{d}l \tag{49}$$

$$\frac{\mathrm{d}l}{\mathrm{d}\alpha} = w(\alpha) l^{-f(\alpha)} \tag{50}$$

$$\sum_i p_i^q \sim \int \mathrm{d}\alpha \, w(\alpha) l^{-f(\alpha)} l^{q\alpha} \tag{51}$$

$$\sim \int \mathrm{d}\alpha \, w(\alpha) e^{\log l (q\alpha - f(\alpha))} \tag{52}$$

The first equation comes because α is defined as the singularity measure, or how much a certain segment $\mathrm{d}l$ contributes to the probability measure, and the second comes about because this is how much each α value contributes to the total probability.

We then use the saddle point approximation to evaluate at $\alpha = a$ where the exponential is maximized, where $q = f'(a(q))$, so that

$$\sum_i p_i^q \sim e^{\log l [q a(q) - f(a(q))]} \tag{53}$$

$$D_q = \frac{1}{q-1} \left[q a(q) - f(a(q)) \right] \tag{54}$$

Typical $f(\alpha)$ are strictly convex $f'' < 0$, and so we see that their maximum occurs at $q = 0, f(\alpha_{\max}) = D_0$. Moreover, $f(\alpha(q))$ vanishes when $q = \pm\infty$, since $f'(\alpha) = q$ is singular there.

11.3 Example multifractal: two-scale factor Cantor set

Consider a similar construction to the Cantor set, but where instead of dropping the middle third of each line segment we keep the initial l_1 and final l_2 of it. Imagine also that for each factor of l_1, we have dynamics with a p_1 probability of visiting, and p_2 probability of visiting each l_2 factor. At the n-th subdivision level there are $\binom{n}{m}$ copies of the line segment with length $l_1^m l_2^{n-m}$ weighted with probability $p_1^m p_2^{n-m}$.

The measure then associated with landing on a particular length segment is $W_{mn} = \binom{n}{m} p_1^m p_2^{n-m}$. Hitting this with Stirling's, we obtain

$$W_{mn} = \exp\left[-\frac{n(m/n - p_1)^2}{2p_1 p_2}\right] \tag{55}$$

which is a sharply peaked Gaussian around width $m/n = p_1$, meaning we will tend to visit line segments with width $m/n = p_1$ with increasing probability as $n \to \infty$.

To compute $f(\alpha)$ from this, we recall that the chance of visiting an interval of length $l_{nm} = l_1^m l_2^{n-m}$ is $p = p_1^m p_2^{n-m}$. But then $p = l^\alpha$, so doing a bit of algebra we can recover

$$\alpha = \frac{\log p_1 + \left(\frac{n}{m} - 1\right)\log p_2}{\log l_1 + \left(\frac{n}{m} - 1\right)\log l_2} \tag{56}$$

f describes the dimension of the set experiencing the singularity α. Thus, the number of intervals must grow like l^{-f}, so $\binom{n}{m} \sim (l_{nm})^{-f}$, which gives

$$f = \frac{\left(\frac{n}{m} - 1\right)\log\left(\frac{n}{m} - 1\right) - \frac{n}{m\log\frac{n}{m}}}{\log l_1 + \left(\frac{n}{m} - 1\right)\log l_2} \tag{57}$$

which along with the above expression for α gives us $f(\alpha)$.

Calculating D_q is hard so I'm not going to think too much about it.

12 Attractor Reconstruction

We've learned many techniques now that are able to identify chaos based on the phase space dynamics, i.e. the attractor. These diagnostics only help when knowing the attractor, and not when knowing only the map, which seems to limit their application to numerical systems.

It turns out however, it is possible to measure a single dynamical variable and construct the phase space attractor in a way that does not destroy the topological diagnostics such as Lyapunov exponents etc.

First, sample a single dynamical variable continuously $x(t)$ at m successive time delays $t + i\tau, i \in [0, m-1]$. Then, construct the vector with components

$$\xi_\alpha(t) = x(t + \alpha\tau) \tag{58}$$

This vector $\vec{\xi}(t)$ is a trajectory in an m-dimensional space, and it turns out that if $m \geq 2D_C + 1$, with D_C the capacity dimension of the attractor, then the trajectory is a faithful reconstruction of the physicas phase space flow. More precisely, the infinitisemal evolution $\delta\vec{\xi}$ in the reconstructed and physical phase space have a ratio that is uniformly bounded and non-vanishing.

Since D_C is not known *a priori*, the usual technique is to sample for increasing m, come back and compute D_C, and see when D_C stops increasing. The extra factor of 2 is to account for possible extra crossings, e.g. embedding a circle in 2 dimensions can be accomplished with two tangent circles (a figure 8), which violates the distance bounds in the faithfulness criterion. In multiple dimensions, the chances that the $\xi(t)$ crosses itself vanishes and so we expect a faithful reconstruction. In practice, sometimes we do not actually care about crossing points, and in that case $m \geq D_C + 1$ is sufficient to represent the trajectory.

The size of τ is actually unimportant in the proof! However, for numerical purposes a τ around the "correlation time" is usually used (the timescale over which the autocorrelation function decays)

13 Bifurcation Theory

A *bifurcation* is when a solution exhibits a change in fundamental character as a control parameter is varied, e.g. when a stable system becomes unstable. In general, it arises because the Jacobian is singular (otherwise, the solution can be analytically continued and is generally expected to exhibit the same behavior).

13.1 Bifurcation from steady-state solution

Consider a system $\dot{U} = f(U|r)$. Call $U = U_0$ a steady state solution $f(U_0|r) = 0$, then we examine the behavior of small perturbations δU about U_0. Linearizing the dynamics

$$K_{ij} = \left.\frac{\partial f^{(i)}}{\partial U^{(j)}}\right|_{U=U_0} \tag{59}$$

$$\delta\dot{U}^{(i)} = K_{ij}\delta U^{(j)} \tag{60}$$

then we find that the eigenvalues λ_α determine the growth rate of perturbations $\delta U \propto \sum_\alpha A_\alpha e^{\lambda_\alpha t} u^{(\alpha)}$ with $u^{(\alpha)}$ the eigenvectors of $\mathbf{K}$ and A_α the components of the initial conditions along these eigenvectors.

Stability requires all $\operatorname{Re}\lambda_\alpha < 0$, which is a function of r. Two possible avenues of change can proceed:

- A single real eigenvalue passes through 0, called a *stationary bifurcation*.
- A pair of complex conjugate eigenvalues passes through the imaginary plane (their real part vanishes). This is called a Hopf bifurcation.

For each of these, as we leave the linear regime, nonlinear behavior takes over and a few possibilities ("normal forms") can arise. We take a look in a moment, but first discuss *bifurcation diagrams*. This is simply a plot of the stationary solutions X as a function of a varied contro parameter r. Stable solutions are represented by solid lines, and unstable by dashed.

13.1.1 Stationary Bifurcations

Transcritical This occurs when the nonlinearity is quadratic, or of the first possible neglected order. For instance, consider $\dot{X} = \epsilon X - X^2$, where we attach an ϵ to the linear term to remind us that we operate in the nonlinear regime.

In this case, we first look for stationary solutions, of which there are two $X = 0, X = \epsilon$. The former is stable for $\epsilon < 0$, the latter the exact opposite. We see that the two solutions "exchange stability" at $\epsilon = 0$.

Pitchfork Often we will see symmetry in the problem $X \to -X$, which makes a X^2 nonlinearity impossible. Thus, we examine systems with the next higher order $\dot{X} = \epsilon X \pm X^3$. The behavior then depends on the sign:

Supercritical ($-X^3$) For $\epsilon < 0$, the only solution is $X = 0$ and no other stable solutions exist, but for $\epsilon > 0$ we have unstable $X = 0$ and two new solutions $X = \pm\sqrt{\epsilon}$ that are stable.

Subcritical ($+X^3$) For $\epsilon < 0$, we have a stable $X = 0$ solution with the two solutions $X = \sqrt{-\epsilon}$ unstable, and for $\epsilon > 0$ we have a single unstable solution at $X = 0$.

Saddle node It is also possible for a normal form that looks like $\dot{Y} = (r - r_0) - Y^2$ with $Y = X - X_0$. The bifurcation diagram for such a normal form looks somewhat like a sideways quartic, where if we sweep r from left to right, we suddenly run into the bottom of the two minima in the quartic. Thus, stable solutions "evolve out of nowhere", and it's only after we get to the "origin" of the quartic (at r_0, X_0) that where the stationary solutions evolve from is clear.

13.1.2 Hopf Bifurcation

With complex eigenvalues, both λ, λ^* must be eigenvalues, and the eigenvector is also complex $Z = |Z| e^{i\phi}$. Notate the eigenvalues $\lambda = \epsilon + i\omega$. There are again two normal forms

Supercritical Of form $\dot{Z} = (\epsilon + i\omega)Z - (1 + ib)\left|Z\right|^2 Z$

We note that for $\epsilon < 0$, we have a stable solution at $Z = 0$, but for $\epsilon > 0$ this solution becomes unstable. Instead, stable solutions develop at $|Z| = \sqrt{\epsilon}, \dot{\phi} = \omega - b\epsilon$, which is simply uiform rotation on a circle. It turns out that to all orders in perturbation theory, the motion is conjugate to motion on a circle.

Subcritical Of form $\dot{Z} = (\epsilon + i\omega)Z + (1 + ib)\left|Z\right|^2 Z$ then only for $\epsilon < 0$ do we incur the circular solutions from the previous part, and they're demonstrably unstable.

13.2 Bifurcation from a Periodic Solution

Let's consider that we have some solution $U_0(t)$ that is peridoic with frequency ω_0. We can determine stability by Floquet analysis: we seek a solution of form

$$U(t) = U_0(\omega_0 t) + e^{\lambda t}\delta U(\omega_0 t) \tag{61}$$

where δU has the same period as U_0. WLOG, assume that $|\operatorname{Im}\lambda| \leq \dfrac{\omega_0}{2}$ because anything higher frequency can be "folded into" δU without changing its period.

While there are the same two types of bifurcations as before, that a real eigenvalue changes signs and that a complex pair of eigenvalues crosses the imaginary axis, but we incur third possibility as a sub-case of the latter: a a complex eigenvalue with $\operatorname{Im}\lambda = \dfrac{\omega_0}{2}$ crosses the imaginary axis: now thanks to the folding procedure above, $\lambda = \lambda^*$!

It's easiest to analyze these possibilities on a Poincaré section, where suddenly our periodic solution becomes a fixed pointt! Consider

$$R_{n+1} = F(R_n|r) \tag{62}$$

Now we just have to look at the Jacobian of this map $\delta R_{n+1} = K\delta R_n$ for some K. But since we have a map, the growth factor isn't $e^{\lambda_\alpha t}$ but instead $(\lambda_\alpha)^n$. We now have three possibilities:

- A real λ passes through $+1$.
- A real λ passes at -1.
- A complex conjugate pair of λ pass through the unit circle.

The first case is uninteresting, a new periodic solution arises that has the same frequency as the original solution (since it lives on the Poincaré section) and stability is determined as usual.

The second case is a bit more interesting. It's evident that at the linear level, new oscillations at $\omega_1 = \operatorname{Im}\lambda$ develop. Nonlinear behavior is complicated. It's possible for frequency locking to occur, depending on the specific frequencies involved, whether hey form an irrational or rational ratio etc. We will come back to this case.

The third case is neat. Any perturbation incurs sign flips on the map, which actually produces *period doubling* in the flow. We can see this by examining the normal form of the Poincaré section map

$$X_{n+1} = -X_n - \epsilon X_n + X_n^3 \tag{63}$$

$$X_{n+2} \simeq X_n + 2\epsilon X_n - 2X_n^3 \tag{64}$$

we see that the only fixed point solution of the every-other-time-tick solution is stable/unstable for ϵ values. Thus, the period of the orbit doubles.

13.3 Quadratic Bifurcations

Recall the quadratic map $f(x) = ax(1-x)$. It turns out that if we plot the Lyapunov exponent λ as a function of a, we see an infinite number of period doubling bifurcations between 3.0 and ≈ 3.57. In other words, for successive bifurcation points a_n, the period doubles to 2^n times the base period.

Similar properties exist for similar maps such as the sine map. What makes these properties somewhat difficult to study is that the dynamics near a bifurcation point are difficult to study, as the Lyapunov exponentent is vanishing.

Instead, it turns out that there exists a value of $a_n^{(s)}$ within each interval $[a_n, a_{n+1}]$ that produces a "superstable 2^n" cycle, such that one point of the orbit is exactly the maximum of the map, and the Lyapunov exponent is exactly $-\infty$.

Let's also demand the separation of points in the orbit as an orbit splits into two at a bifurcation point. Specifically, for a superstable 2^n orbit, it's noted that the maximum point exhibits the smallest splitting between itself and the point halfway around the orbit. Call this separation d_n.

It turns out that the separation between the $a_n^{(s)}$ decrease geometrically, as do the d_n. We can then compute these ratios as $n \to \infty$.

It turns out interestingly that these ratios hold true for the sine map $f(x) = \frac{1}{4}a\sin(\pi x)$ as well, the *exact same ratios*. It turns out that all maps with a quadratic maximum yield the same ratio!

Let's develop some notation for this. Consider an arbitrary map $f(x)$, and call f^n its nth functional composition. Denote x_0 a fixed point of $f(x)$. Then it turns out that

- The stability of a fixed point is determined by the slope of $f(x = x_f)$. If $|f'(x_f)| < 1$, then perturbations shrink and we have a stable fixed point, else unstable (just like our analysis with K above except K is a scalar). Period doubling bifurcations correspond to $f'(x_f) = -1$.

- Then, as some control parameter crosses from stable to unstable, we note that $\left.\dfrac{\mathrm{d}f^2}{\mathrm{d}x}\right|_{x=x_f} = +1$, and moreover changes in magnitude from < 1 to > 1.

Moreover, for $a < a_c$ the critical a, we find that f^2 must also have effective slope less than unity (I mean for instance that f^2 stays below $y = x$, the line of slope 1, for $x > x_f$). Then, as we cross the critical a_c, the slope of f^2 at x_f increases to be above 1. But in order to maintain continuity of f^2, as the rest of it is still "below" $y = x$, it is clear that f^2 must cross $y = x$ again, this time with a slope < 1.

Thus, we see that for these bifurcations where a stable fixed point becomes unstable, two new stable fixed points must arise. But these two new fixed points cannot be fixed points of f, only of f^2, and so manifestly f flips them back and forth (more precisely, (x_1, x_2) are the points of a period 2 orbit of f).

14 Renormalization Group Theory

Renormalization is all about "functional composition and rescaling." Let's again examine the quadratic map, but this time make a small coordinate shift $x \to x - \frac{1}{2}$. Let's now examine the following functional operator

$$T_\alpha[f(x)] = -\alpha f\left(f\left(-\frac{x}{\alpha}\right)\right) \tag{65}$$

It is then clear that

- For particular α, T has a fixed point solution $g(x)$, e.g.

$$g(x) = -\alpha g\left(\left(-\frac{x}{\alpha}\right)\right) \tag{66}$$

  As in linear algebra, there is a family of g that satisfy the above, so we fix the "normalization" and require $g(0) = 1$. Otherwise, if $g(x)$ is a solution then so too is $\mu g(x/\mu)$.

- It turns out that linearizing T about the fixed point $g(x)$ yields a *single* unstable eigenvector with eigenvalue δ.

  More precisely, if we let $f(x) = g(x) + \varepsilon(x)$, then let's define linearized operator $L[\varepsilon] = T[g + \varepsilon] - T[g]$, and define $\lambda^{(i)}, \varepsilon^{(i)}$ eigen-thingies sorted in descending order by the λ to be such that

$$L[\varepsilon^{(i)}(x)] = \lambda^{(i)}\varepsilon^{(i)}(x) \tag{67}$$

  then per our above claim $\lambda^{(1)} = \delta > 0$ and the other $\lambda^{(i)}$ are all negative.

More interestingly, it turns out that α, δ are fixed values *independent* of T, g.

Examine the first powers of $g(x) = 1 + bx^2$, then

$$g(x) = g\left(g\left(-\frac{x}{\alpha}\right)\right) \tag{68}$$

$$= 1 + b\left(1 + b\frac{x^2}{a^2}\right) \tag{69}$$

$$1 + bx^2 = -\alpha\left[1 + b + x^2\left(\frac{2b^2}{\alpha^2}\right)\right] \tag{70}$$

which forces $\alpha = 1 + \sqrt{3}, b = -\frac{\alpha}{2}$ (b must be negative since $g(x)$ is convex).

δ is fixed by literally approximating $g(x) = 1$ and mandating that the linearized L of operator T be satisfied at $x = 0$, which produces $\delta = \alpha^2 - \alpha \approx 4.73$.

More precise values than the above can be obtained, but these approximations serve to show that the above two observations alone constrain the effect of T with no knowledge of any physical system!

Now, let's call the single expanding eigenvector (with eigenvalue δ) h. Then let's examine a class of solutions

$$g_r(x) = g(x) + \delta^{-r}h(x) \tag{71}$$

with h the eigenvector and r a large number. Then we find that

$$T[g_r(x)] \approx g_{r-1}(x) \tag{72}$$

when we linearize about $g(x)$.

Let's apply our intuition from discrete maps for a moment. Suppose $g(x)$ is thought of as a map and has a stable 2^n cycle, then $g(g(x))$ must have a stable 2^{n-1} cycle. Thus, we see that composition of the g serves to halve the period, and so $T[g(x)]$ serves equally to halve the period (since it's just a constant multiple of a functional composition). Thus, we see that each $g_r(x)$ can be thought of as having period 2^r.

For convenience's sake, let's terminate the series at some g_0. This isn't explained well in the lecture notes, but I imagine this to be the most basic solution, e.g. the

SHO solution or the period 1 solution. It's understandable that such a "unit time solution" should exist, but what happens when we operate on it with T is beyond me...

14.1 Bifurcations in the physical map

What about the rest of the function space? Since there is a single unstable direction about $g(x)$, we see that there must exist a "stable manifold" for which repeated iteration of T brings all functions to $g(x)$ the fixed point. This manifold is expected to have codimension 1 (I envision this as a space orthogonal to the unstable $h(x)$ direction). Then, for a family of functions $f_R(x)$ parameterized by a single value R, we might expect for a single value of R for $f_R(x)$ to live in this stable manifold. Define this single value of R to be R_∞, then we would have $n \to \infty, T^n f_{R_\infty} \to g(x)$.

Now, what about f_R for R *near* R_∞? We would expect repeated iteration of T to bring us very close to the fixed point, tracking the f_{R_∞} evolution, until eventually the nonzero component along $h(x)$ kicks in. This is the point at which we must be careful. Let's examine the evolution in steps:

- First, we evolve a finite q number of times to bring $T^q f_R$ into the "vicinity" of the fixed point. In general, so long as $R - R_\infty$ is a small number, q is fixed; it's however long it takes for f_{R_∞} to come close to the fixed point.

  Next, we might ask how big the $h(x)$ component is after q iterations. Taylor expanding. It might be a bit difficult to determine *a priori*, so let's just call this component $\bar{c}(R - R_\infty)$. Thus we can notate

  $$T^q f_R = g(x) + \bar{c}(R - R_\infty)h(x) \tag{73}$$

- Next, we evolve some p number of times such that the function is dominated by the $h(x)$ component but still such that the linearization holds. Naturally, since $\bar{c}(R - R_\infty)$ should be a roughly proportional function of $R - R_\infty$, we will see an inverse proportionality between $p, \bar{c}(R - R_\infty)$, since we'll "need more iterations to leave the domain where linearization holds."

- Finally, we complete T^n iterations with a further $n-p-q$ iterations which is expected to take us into the nonlinear regime.

Using this highly qualitative terminology, we can rewrite

$$T^n f_R = T^{n-p-q}\left[g(x) + \bar{c}(R-R_\infty)\delta^p h(x)\right] \tag{74}$$
$$= T^{n-p}\left[g(x) + c(R-R_\infty)\delta^p h(x)\right] \tag{75}$$

where we redefine $c(R-R_\infty) = \bar{c}(R-R_\infty)\delta^q$ for simplicity.

Let's now make special choices of $R = R_m$ such that $c(R-R_\infty) = \delta^{-m}$, then we instead obtain

$$T^n f_{R_m} = g(x) + T^{n-p}\delta^{p-m}h(x) \tag{76}$$
$$= g_{m-n} \tag{77}$$

where g_{n-m} is just the g_r we discussed earlier. Since we saw earlier that T acts on these functions by simply changing the index (and the period), we find that f_{R_m} must also have a 2^m cycle.

Phew, this was a mounthful, what does it all amount to? We've shown that universal to all maps T satisfying the assumed two properties from the beginning of this section, period doubling cascades show up. In this particular case, the cascade appears as $R_\infty - R_m \to 0$, and the period doubles without bound. Moreover, since we only need a stable manifold with codimension 1 for this cascade to happen, this should be a reasonably common occurence.

14.2 Rescaled maps

Let's fiddle a bit more:

$$f^{2^n}(x) = (-\alpha)^{-n} T^n f\left((-\alpha)^n x\right) \tag{78}$$
$$f_{R_m}^{2^n}(x) = (-\alpha)^{-n} g_{m-n}\left((-\alpha)^n x\right) \tag{79}$$

In particular, if we take $m = n$ then

$$\lim_{n\to\infty} f_{R_m}^{2^n}(x) = (-\alpha)^{-n} g_0((-\alpha)^n x) \tag{80}$$

where $g_0(x)$ is the first in the g_r series we studied earlier. We can converge to any of the g via this rescaling procedure by appropriate choice of m. Moreover, if we start from $R_m = R_\infty$ instead, we get g the universal stable point $g(x)$.

There's a chapter here that concerns "advanced topics" but I forgo this for my sanity. Some notable points include an analysis of the power spectrum of the period doubling route to chaos (subharmonic peaks appear as well as a broad band), a structure of the dynamics (regular frequency bands but random jumping within each band), and behavior in the presence of noise (higher frequencies are attenuated, thus chaos onsets earlier).

15 Driven Pendulum and 2D circle map

One common route to chaos is the breakdown from a quasiperiodic state of n discordant frequencies, which looks like an n-torus. It might be expected that, similar to period doubling, an n-torus must go to a more complex torus before it can reach a chaotic state. It turns out that's not always the case.

15.1 Driven Pendulum

Consider the EOM

$$\ddot{\theta} + \gamma\dot{\theta} + \sin\theta = d + g\cos\omega_D t \tag{81}$$

which is just a running oscillation with a fixed nonzero $\left\langle \dot{\theta} \right\rangle$. Frequency locking can then occur between $\omega_D, \left\langle \dot{\theta} \right\rangle$.

Let's turn this into a flow in 3D space

$$\dot{\theta} = \omega \tag{82}$$

$$\dot{\omega} = -\gamma\omega - \sin\theta + d\cos\theta_D \tag{83}$$

$$\dot{\theta_D} = \omega_D \tag{84}$$

Or we can turn it into a 2D map by strobing at ω_D and plotting (θ, ω). The exact form of the mapping function is complicated, given that it is the integral of the flow, but examining the Jacobian we find that it is equal to $J = e^{2\pi\gamma/\omega_D} < 1$, so the map uniformly contracts.

15.2 Periodically kicked rotor

Quantitative study of the above is complicated, since we'd actually have to quantitatively state the reduction of the flow to the map. Instead, let's consider a simpler

example, where we have a SHO that is periodically kicked

$$\ddot{\theta} + \gamma\dot{\theta} = (A - B\sin\theta)\sum_n \delta(t-n) \tag{85}$$

The plus is that the motion is easily integrable between kicks, since it's just a free SHO then. Integrating and strobing at $t = n$, we find

$$\theta_{n+1} = \theta_n + \frac{1-e^{-\gamma}}{\gamma}\left(\dot{\theta}_n + A - B\sin\theta_n\right) \tag{86}$$

We can then make a couple of definitions and obtain

$$\Omega = \frac{A}{2\pi\gamma}, r_n = \frac{e^{\gamma}-1}{\gamma}\dot{\theta}_n - 2\pi\Omega, \frac{K}{2\pi} = \frac{1-e^{-\gamma}}{\gamma}B, b = e^{-\gamma} \tag{87}$$

$$\theta_{n+1} = \theta_n + 2\pi\Omega - K\sin\theta_n + br_n \tag{88}$$

$$r_{n+1} = br_n - k\sin\theta_n \tag{89}$$

The determinant of the Jacobian is b, so areas contract if $b < 1$.

Then there are demonstrations. Welp. I guess this lecture just introduced a couple of systems. Don't think I can do these demonstrations though since I don't know what to examine.

16 Circle Map

The one dimensional circle map is given by

$$x_{n+1} = x_n + \Omega - \frac{K}{2\pi} \sin 2\pi x_n \tag{90}$$

which is then mapped back to the unit interval by a modulus operator. We define the winding number

$$W = \lim_{n\to\infty} \frac{x_n - x_0}{n} \tag{91}$$

to be the average number of rotations around the unit interval that x performs.

16.1 $K < 1$

For $K < 1$, we observe monotonic, invertible growth. We observe a couple of properties:

- The winding number is either rational (corresponding to locked motion at the frequency of the stobing) or irrational (corresponding to unlocked motion e.g. quasiperiodic).
- W is a continuous function of Ω. It exhibits a structure that is shown below in Figure 1.
- The sum of the widths of the rational steps in the figure above tends to 0 for $K \to 0$ and to unity as $K \to 1$. Interestingly, these rational steps are known as "Arnold tongues."

16.2 $K = 1$

- At $K = 1$, the map develops an inflection point at $x = 0$.
- The measure of Ω giving irrational W is 0, as the sum of the widths of the rational steps is 1 from above. It turns out the set has fractal dimension 0.87.

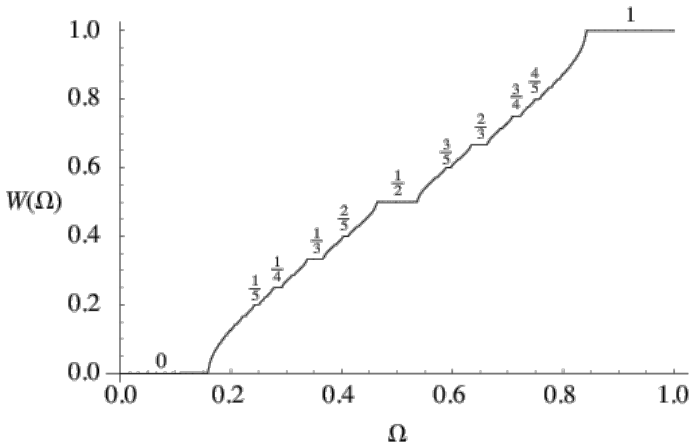

Figure 1: A plot of $W(\Omega)$ grabbed from `http://mathworld.wolfram.com/DevilsStaircase.html`.

- Since passing through the inflection point yields chaos, and irrational winding number solutions tend to visit every point on the interval, irrational winding number solutions break down to chaos at $K = 1$.
- Since rational winding number solutions visit a discrete number of points of the map, they tend not to break down to chaos.

16.3 $K > 1$

- The Arnold tongues may overlap, which produces hysteresis.
- The map has a quadratic maximum, and similar to the quadratic map even periodic solutions can break down to chaos via period doubling cascades.

17 Universal Onset of Chaos from a 2-torus

We will adopt a similar approach to that used for the circle map for a quasiperiodic torus, but the best way to examine the problem isn't to increase K for fixed Ω, but rather to increas for fixed winding number W. This makes the theory a bit more difficult, but let's sketch the argument here.

For any quasiperiodic orbit, we must examine irrational winding numbers. We will formulate our plan of attack with a series of rational approximations, the theory for which is founded in the theorem that any irrational number can be uniquely written in a continued fraction expansion. Truncating this continued fraction at the nth level gives the nth rational approximant W_n to irrational W.

Just a curious fact before we continue: define integers $(a_1, a_2, \dots)$ to be the integers in the continued fraction

$$W = \cfrac{1}{a_1 + \cfrac{1}{a_2 + \cfrac{1}{\cdots}}}, \tag{92}$$

then it turns out that all solutions to quadratic equations have periodic rational expansion $(a_1, a_2, \dots)$. Moreover, the Golden mean $\dfrac{\sqrt{5}-1}{2}$ corresponds to $(1, 1, \dots)$, which produces the slowest converging rational expansion. The silver mean donetos $\sqrt{2} - 1$, which corresponds to $(2, 2, 2 \dots)$.

We will first motivate the discussion with some numerical results for the circle map, then study the renormalization group theory for this system.

17.1 Circle Map Results

- Define G_n the nth rational approximation to the golden mean, then $\Omega_n(K)$ is the value of Ω for a given K that produces winding number G_n. This results in the trajectory $f_{K,\Omega_n}^{F_{n+1}}$. We can then find that

$$\lim_{n\to\infty} \Omega_n(K) = \Omega_\infty(K) - c\tilde{\delta}^{-n} \tag{93}$$

where $\Omega_\infty(K)$ produces winding number G the golden mean itself, and

$$\tilde{\delta} = \begin{cases} G^{-2} = 2.618\ldots & K < 1 \\ 2.8336\ldots & K = 1 \end{cases} \tag{94}$$

where the $K < 1$ case can be determined simply by looking at uniform rotation, but the $K = 1$ must be computed numerically.

- The distance d_n from $x = 0$ to the nearest other element of the G_n cycle scales as

$$\frac{d_n}{d_{n+1}} \to \tilde{\alpha} \tag{95}$$

with

$$\tilde{\alpha} = \begin{cases} -G^{-1} = -1.618\ldots & K < 1 \\ -1.28857\ldots & K = 1 \end{cases} \tag{96}$$

- Note that $\tilde{\delta}, \tilde{\alpha}$ are universal to all maps for a given winding number.

17.2 Renormalization

Since we notice that the point separation has some nice scaling structure, let's renormalize the orbits. Define

$$\bar{f}^n(x) = f^{F_{n+1}}(x) - F_n \tag{97}$$

and the scaled

$$\bar{f}_n(x) = \tilde{\alpha}^n f^{F_{n+1}}(\tilde{\alpha}^{-n}x) - F_n. \tag{98}$$

These functions exhibit the property

$$\bar{f}^{n+1}(x) = \bar{f}^{n}\left(\bar{f}^{n-1}(x)\right) \tag{99}$$

We now look for a fixed point structure, i.e. a function $\bar{f}^*$ satisfying

$$\bar{f}^*(x) = \tilde{\alpha}\bar{f}^*\left(\tilde{\alpha}\bar{f}^*\left(\tilde{\alpha}^{-2}x\right)\right) \tag{100}$$

One such solution is $\bar{f}^*(x) = x + C$, which gives $\tilde{\alpha} = -G^{-1}$. When $K = 1$, the linear term disappears, and a second solution with the numerical $\tilde{\alpha}$ appears. We can perform this analysis by linearizing about the fixed point.

18 Ruelle-Takens Theorem

The Ruelle-Takens Theorem, later extended with Newhouse (henceforth referred to as RTN), was initially misunderstood due to its highly mathematical language but is still very useful. It concerns whether chaos arises from accumulation of bifurcations or whether low-dimensional chaos is an additional route to chaos. Its statement follows:

Let v be a constant vector field on the torus $T^n = R^n/Z^n$. If $n \geq 3$ then every C^2 neighborhood of v contains a vector field v' with a strange *Axiom A* attractor. If $n \geq 4$ we may take C^∞ instead of C^2.

That's a mouthful. Can we clarify a bit?

- For a set of ODEs $\dfrac{\mathrm{d}\vec{x}}{\mathrm{d}t} = \vec{v}(\vec{x})$, we call $\vec{v}(x)$ the vector field that generates the flow $\vec{x}(t)$.
- A constant vector field on an n-torus corresponds to uniform rotation in each of the n directions, generally quasiperiodic.
- C^2 refers to twice differentiable, C^∞ means smoothl/infinitely differentiable.
- An *Axiom A* attractor is an attractor with many nice properties such as robustness under small parameter changes.

Thus, the RTN theorem says that it's possible to make certain arbitrarily small perturbations to turn motion from an quasiperiodic $n$torus to chaotic for $n \geq 3$. However, the chaotic motion remains *on* the torus, and is robust to further arbitrarily small perturbations. The "every" neighborhood refers to the fact that all points in the vector field have such perturbations, but not that a generic perturbation effects chaos. This was a stumbling point in early use/interpretation of the theorem.

We do some numerical investigations of the theorem to illustrate precisely this point, that a system that moves beyond linear dynamics is equally likely to break down to period locked motion as to chaos.